SUPERALLOY POWDER PROCESSING, PROPERTIES AND TURBINE DISK APPLICATIONS

D.R. Chang, D.D. Krueger, R.A. Sprague

General Electric Company
Aircraft Engine Business Group
Cincinnati, Ohio 45215
USA

Abstract

This paper discusses the characteristics of inclusions resulting from various consolidation techniques and their effects on the fatigue properties of a typical high-strength PM superalloy, Rene' 95. The nature, origin, and size range of defects found in HIP, HIP + isothermally forged, extruded + isothermally forged material are described and their influence on LCF behavior analyzed. Thermomechanical processing improves the LCF life considerably. The improvement is attributed to the dispersion of large defects. The LCF life of forged material is also benefited by a greater tendency toward internal fatigue initiation at crystallographic origins or initiated at smaller defects. The effects of heat treatment on the mechanical properties and microstructural features of extruded + isothermally forged materials are also investigated.

Introduction

The demand for improved jet engine efficiency and performance has resulted in the continued development of high strength disk superalloys, such as Rene' 95. Concurrent with the increase in strength is a significant decrease in conventional hot workability. The decrease in workability adversely affects the overall component cost and the ability to achieve desirable properties. This has spurred the development of powder metallurgy (PM) techniques for producing components of highly alloyed compositions to achieve the desired microstructures, properties, and cost effectivity.

While PM processing provides property and cost advantages over cast and wrought processing, the low cycle fatigue (LCF) capability of PM materials has been limited by the presence of inclusions. These inclusions or defects are introduced during various processing steps. Their nature, size, and distribution are dependent on the PM consolidation technique. PM superalloys can be consolidated by hot isostatic pressing (HIP), HIP followed by isothermal forging (H+F), extrusion (EX), EX followed by isothermal forging (EX + F) or other combinations of compaction and working. A thorough knowledge of the effect of consolidation on defect characteristics is essential for process improvement, material behavior understanding, and hardware performance prediction.

This paper describes the defects which have been induced or are naturally occuring in PM Rene' 95 consolidated by various techniques. An emphasis is placed on the analyses of defect morphologies and their relationship to LCF behavior. For purposes of this paper, a defect is defined as any material heterogeneity which results in a failure mode at the origin by any mechanism other than crystallographic initiation. In addition, the microstructure and mechanical properties resulting from various consolidation techniques and heat treatments are discussed.

Materials and Processing

PM Rene' 95 has a nominal composition (in weight %) of 0.065C, 13Cr, 8Co, 3.5Al, 2.5Ti, 3.5Cb, 3.5Mo, 3.5W, and balance Ni. It normally consists of primary, intermediate, and fine gamma prime (γ') in a highly alloyed gamma matrix which also contains a fine dispersion of Cb, Ti-rich carbides. The materials discussed in this paper were produced from ~150 mesh argon atomized powder. The consolidation techniques considered include HIP, H+F, EX, and EX+F.

The HIP material was consolidated with a 2050°F/15 KSI HIP cycle. The heat treatment consisted of a 2065°F/1 Hr., oil quench solution, followed by a 1600°F/1 Hr. plus 1200°F/24 Hrs. air cool age cycle. The typical microstructure, shown in Figure 1a, has an average grain size of ASTM 8 to 10. Transmission Electron Microscopy (TEM) has been used to study the γ ' and dislocation features[1]. The primary γ ', located at grain boundaries, is generally on the order of 1 micron in diameter. Intermediate and fine γ', located in the grain interiors, typically measure 0.5 and 0.1 microns in size respectively. Both of these γ ' particles have a roughly spherical morphology while the primary γ ' have a blocky shape. An array of misfit dislocations usually surrounds the intermediate γ '. Some dislocations also exist in matrix regions
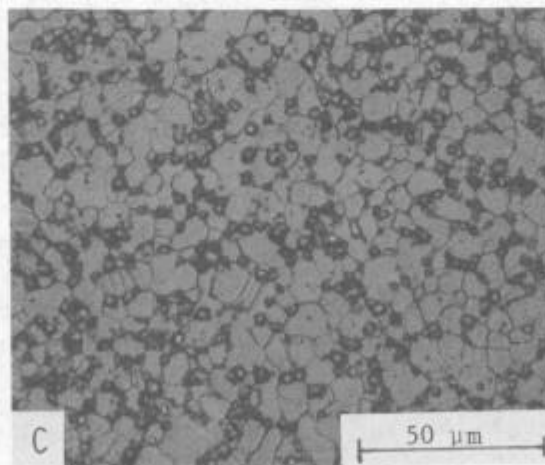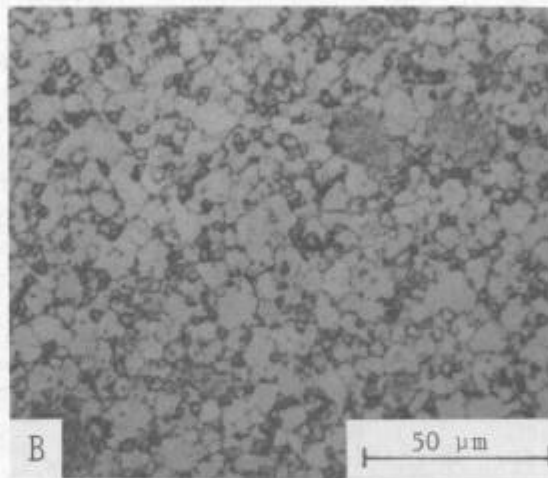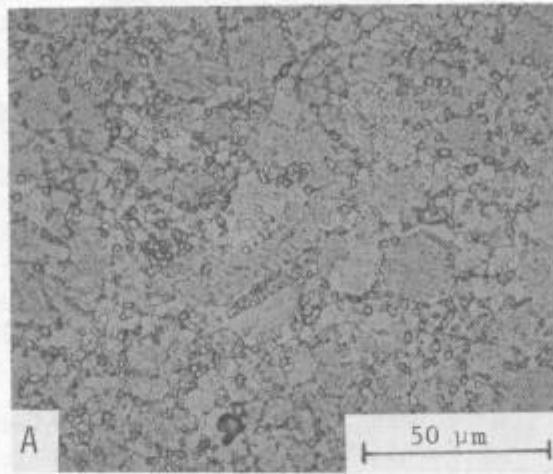
Figure 1 - Optical micrographs showing
typical fine grain microstructures of
HIP (A), H+F (B), and EX+F (C) P/M Rene' 95.

between the intermediate γ '. These are generally found in a random array although distinct slip bands, in rare instances, have also been observed. There is no indication of interaction between the matrix dislocations and fine γ '. Figure 2a shows a TEM thin foil micrograph which illustrates the dislocation distribution near and between intermediate γ ' particles.

The H+F material was produced by isothermal forging of HIP preforms at temperatures between 2000°F and 2050°F. The forging height reduction was nominally 70 to 80%. This material was solutioned at 2050°F for 1 hour, air cooled and aged at 1400°F for 8 to 16 hours. H+F Rene' 95 has a uniform recrystallized grain structure with an average grain size of ASTM 10 to 11. The typical microstructure is shown in Figure 1b. The EX+F material was isothermally forged and heat treated similarly to the H+F material. The preform in this process was consolidated by hot extrusion with a nominal 6.5 to 1 reduction in cross section area. The microstructure of EX+F materials, shown in Figure 1c, is similar to that of H+F material. The γ ' and dislocation features of EX+F Rene' 95 have also been studied[1]. Relative to HIP Rene' 95, this material showed somewhat larger (1-2 microns in diameter) and more frequent primary γ ', smaller intermediate γ ' (0.2-0.3 microns in diameter) and fine γ ' having a similar size. The fine γ ' also exhibited a spherical morphology while the intermediate γ ' was cuboidal rather than spherical. Some differences in the dislocation network were also observed. No misfit dislocations surrounded the intermediate γ ', and the matrix dislocations showed a very heterogeneous distribution between grains. In grains of high dislocation density, the matrix dislocations were localized between the intermediate γ ' particles and showed a tendency to form bands along crystallographic directions. Occasional sub-grain boundaries were also observed. Figure 2b shows a TEM micrograph which illustrates the cuboidal morphology of the intermediate γ ', lack of misfit dislocations near these particles, and the banding of matrix dislocations typically observed.

## Defect Characterization and Effect on Low Cycle Fatigue

HIP PM Rene' 95 Defects

PM defects have been extensively studied for HIP consolidated Rene' 95. This experience has largely resulted from a large scale study of LCF specimen fatigue origins[2][3]. Table 1 summarizes the characteristics of four types of defects found at the failure initiation sites of HIP Rene' 95 LCF specimens.

Type 1 and 2 defects are illustrated in Figure 3. These defects are ceramic inclusions. Type 1 exist as discrete and often chunky particles while Type 2 are agglomerates of fine particles. Both types originate from the melting crucible, pouring tundish or the atomizing nozzle. Aluminum is usually the major metallic element with Zr, Mg or Ca also present in various amounts. The amount of minor elements depends on the type of ceramic involved. The sizes of Type 1 and Type 2 defects are limited by the screen opening through which the powders have been sieved and are not altered significantly by reaction during the HIP cycle. As indicated in Table I, the ceramic defects average about 10 mils^2 with very few reaching 50-100 mils^2.
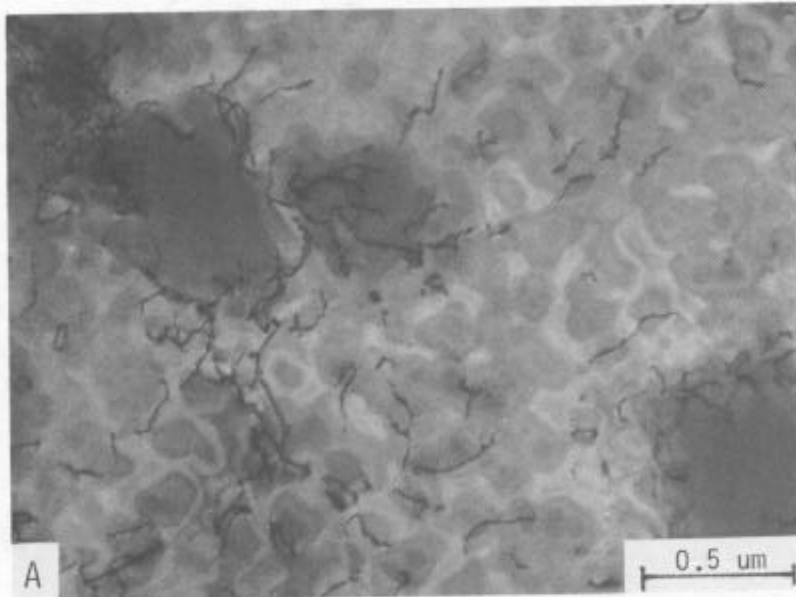
A) HIP PM Rene' 95
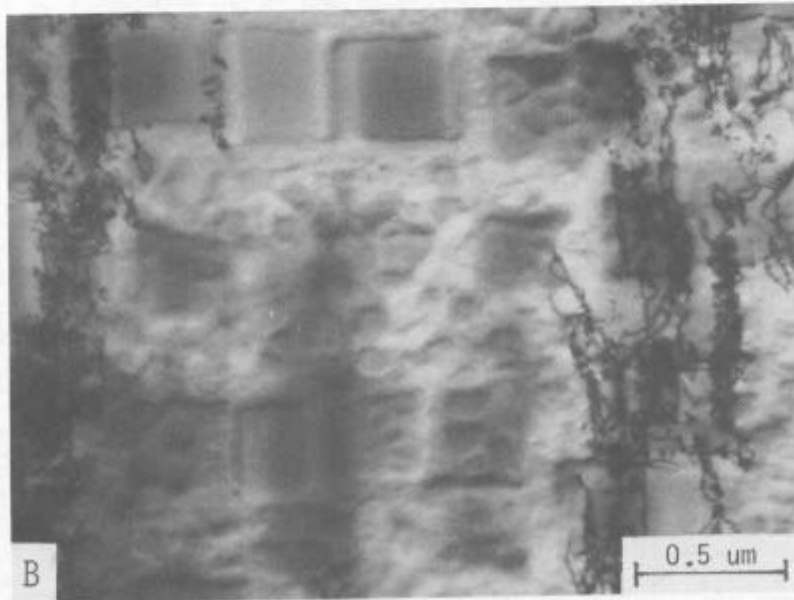
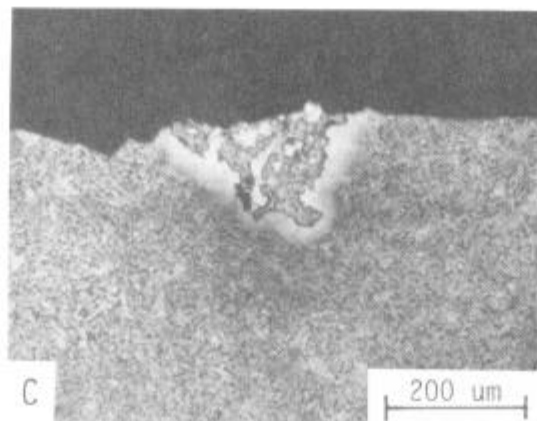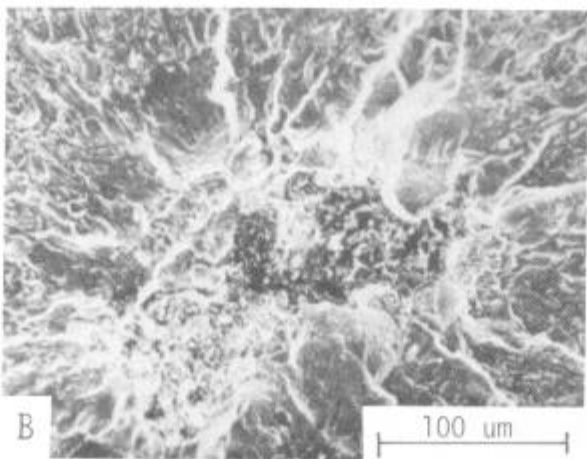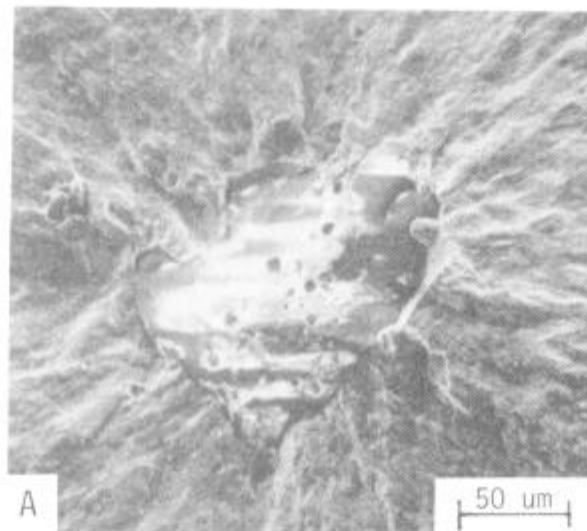B) EX+F PM Rene' 95

Figure 2 - TEM micrographs of PM Rene' 95.

Figure 3 - Micrographs showing ceramic defects.

A) Type 1 SEM fractograph showing fatigue initiation site

B) Type 2 SEM fractograph showing fatigue initiation site

C) Type 2 Optical micrograph from metallographic section

Table I. Major Types of Defects in HIP Rene' 95

Type	Description	Typical Elements	Size, Mils^2(*) Avg.	Max.
1	Discrete chunky ceramic	Al, Mg, Zr, Ca, O	8	50
2	Ceramic agglomerates	Al, Si, Mg, Ca, O	10	110
3	Reactive agglomerates forming PPB	Al, Zr, Cr, Ca, O C, Ca, Fe	15	250
4	Voids	Ar	$\angle 2$	--

(*) Based on defects at initiation sites of LCF test
specimens made from -150 mesh powder(3).

Type 3 or Prior Particle Boundary (PPB) defects are "diffused" and generally occupy a much larger volume of material than Type 1 or 2 defects. As shown in Figure 4, Type 3 defects are characterized by a semi-continuous network of fine oxide or carbide particles around the host powder surfaces. A residual core of the initial contamination source may be present at center of the affected area. Figure 4a illustrates an example of a PPB defect with a core of refractory remaining. PPB defects also exhibit a ballular feature as shown in the fatigue origin fractograph of Figure 4b. Formation of Type 3 defects appears to require a source of oxygen or carbon which reacts with powder surfaces during the HIP cycle. Potential sources of PPB defects include refractory binder (sodium silicate), organic contaminants (Buna N, rubber, and vacuum grease), and mill scale (rust). Depending on the nature and amount of the contaminant, PPB defects can range from several mils^2 to orders of magnitude larger than the maximum size of 250 mils^2 shown in Table I. Consequently, PPB defects are the most detrimental to the properties of PM superalloys.

Since the powders are produced by argon atomization, argon is occasionally entrapped in the powder particles, giving rise to voids or Type 4 defects. An example of a Type 4 defect is shown in Figure 4c. These defects seldom exceed 2 mils^2.

Effects of Defects on HIP Rene' 95 Low Cycle Fatigue

Defects are of major concern to PM superalloys primarily because of their adverse effect on LCF. The total LCF life (N_f) of high-strength disk alloys can be considered to consist of three parts: life spent in crack initiation (N_o), life in Stage 1 propagation (N_I) and life in Stage 2 propagation (N_{II}) which ends in final failure.
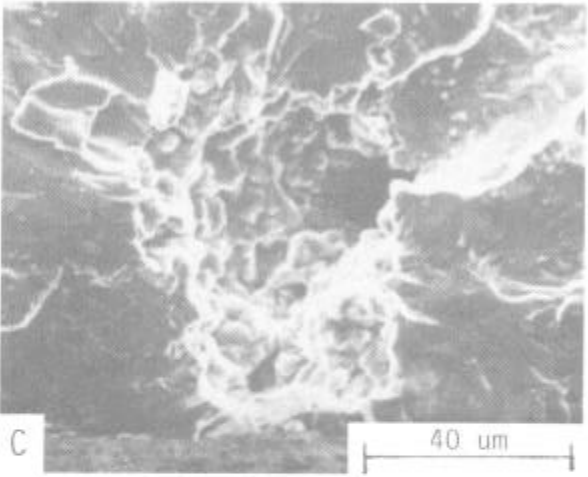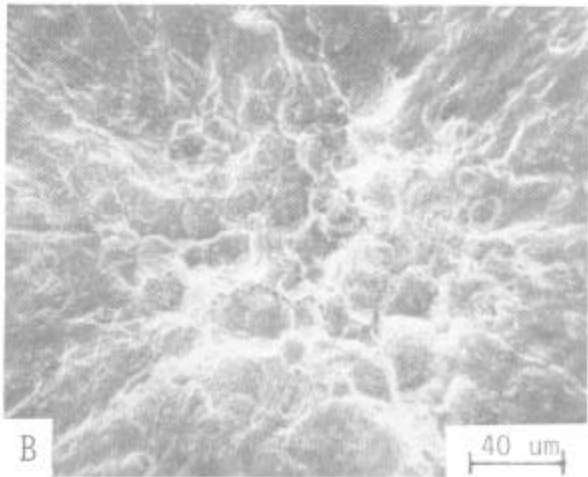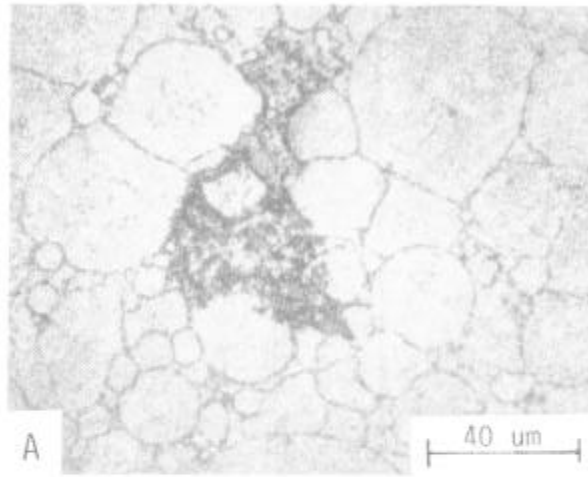
Figure 4 - Micrographs showing:

A) Type 3 (PPB) Optical micrograph from a
    metallographic section

B) Type 3 (PPB) SEM fractograph showing
    fatigue initiation site

C) Type 4 (void) SEM fractograph showing
    fatigue initiation site

The effect of defects on LCF life depends on defect size and defect location in the LCF specimen. This is illustrated in Figure 5 for HIP Rene' 95 tested at 1000°F for a total strain range ($\Delta\varepsilon_t$) of 0.66% and alternating/mean strain ratio (A) of 1. The data shown were obtained from specimens which contained either surface or internal defects. Note that for a given size, a defect is much less detrimental when situated internally than when it is located at the surface. The less severe effect of internal defects is largely due to the absence of adverse environmental interactions. Work performed by Henry[4] has shown that fatigue properties under the absence of an adverse environment are significantly better than similar tests in air. Other investigations have shown this to be a trend for many structural materials [5][6]. Figure 5 also shows that the LCF life of HIP PM alloys can be improved by reducing the size and quantity of defects. This concept is particularly pertinent to PPB type defects.
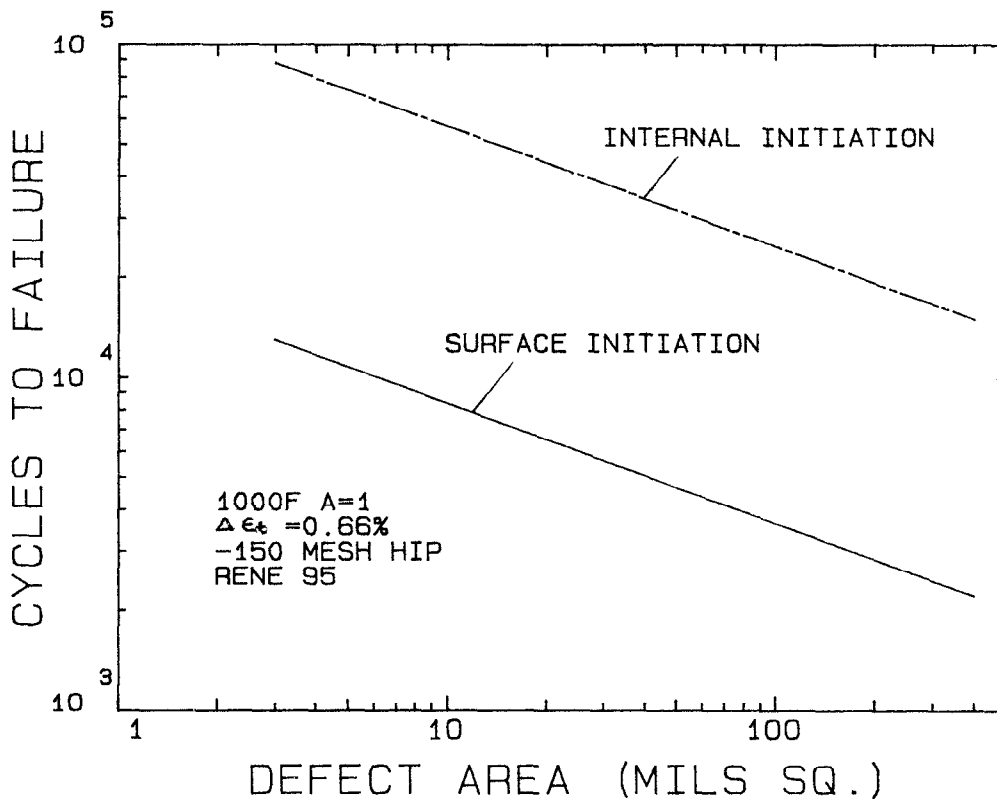

Figure 5 - Effect of defect size and failure location on HIP Rene' 95 LCF life.

Effect of Thermomechanical Processing on Defects

Doped Materials

Typical -150 mesh HIP Rene' 95 material consists of more than six billion original powder particles per pound. The frequency of large reactive defects (PPB) in HIP Rene' 95 was found at a very low level of one in every 1.5 trillion powder particles. This calculation was based on vast hardware inspection experience using extremely sensitive ultrasonic inspection techniques. In order to study the effect of thermomechanical processing (TMP) on defects and properties, Rene' 95 was purposely doped with contaminants to increase the frequency of observance.

Chang et. al[3] have shown that when doped HIP Rene' 95 was isothermally forged, the large reactive type (PPB) defects were dispersed and reduced, while little effect was observed on Type 1 chunky ceramic inclusions. The dopants selected were Al_2O_3 (Type 1, -60 +80 mesh, 1000 particles per pound), Buna N (O ring material, Type 3, 500 particles per pound) and vacuum grease (Type 3, 1cc per pound). The materials were HIP'd at 2050°F and isothermally forged at 2050°F to an 80% reduction. As can be seen in Figure 6 the larger PPB defects were greatly reduced in size and dispersed into stringer shapes. The dopants in HIP material reduced both tensile ductility and LCF life as shown in Table II. Consistent with the defect modification, TMP improved both tensile ductility and LCF life.

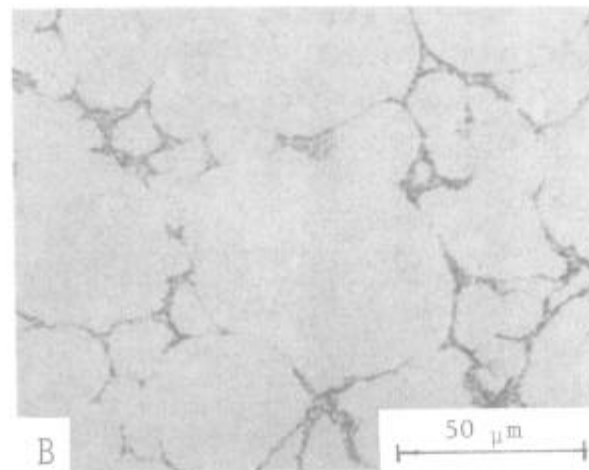Table II. Effect of Isothermal Forging on Ductility and LCF Life of Seeded Rene' 95 (Ref. 3)

Material	RT/1200F Tensile % Elong.	1000F/0.66% $\Delta \epsilon_t$ LCF Life, Cycles Average
1. HIP (Unseeded)	17/15	36,840
2. H+F (Unseeded)	20/22	128,848
3. HIP (Al_2O_3 Seeded)	10/5	3,411
4. (3) + F	14/15	8,219
5. HIP (Buna N Seeded)	10/3	2,561
6. (5) + F	19/19	134,001

* All -150 mesh powder. Forging reduction: 80%

A similar study was conducted to investigate the effect of extrusion and extrusion plus isothermal forging on defects. Since the primary concern was for large reactive defects, two PPB forming dopants were selected; Buna N,(an organic carbide type former) and mill scale (an inorganic oxide type former). These two dopants were separately introduced into Rene' 95 powder which was then processed to produce HIP, EX, and EX+F materials. The extrusion was processed with a nominal 6.5 to 1 area reduction ratio. Isothermal forging resulted in a 60%
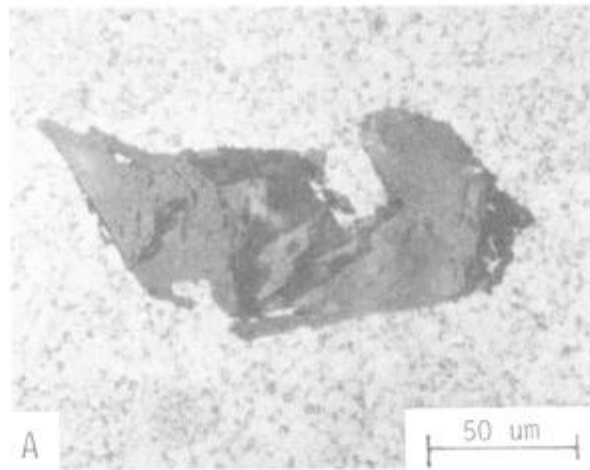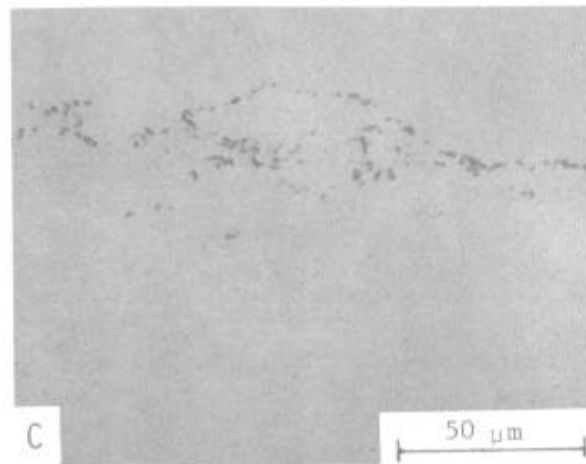
Figure 6 - Optical micrographs showing
effect of isothermal forging on defects
and LCF failure initiation in H+F
Rene' 95:
A) Alumina inclusion in H+F
B) Vacuum grease induced PPB in HIP
C) PPB modification by 80% forging
    reduction

reduction in height. The HIP material showed many PPB defects with some as large as 1200 mil^2. It is evident from Figure 7 that both EX and EX+F greatly reduced and dispersed the reactive defects. In addition, Figure 8 shows that TMP has destroyed the ballular nature of PPB defects and generated a recrystallized zone around the core.

As a result of defect modification, the tensile ductility and LCF of doped EX+F Rene' 95 were improved significantly as shown in Tables III and IV. The defects at the fatigue origins were also characterized. As can be seen from Table III and Table IV, 90% of the doped HIP Rene' 95 specimens failed from PPB, while no PPB origins were found in the doped EX+F material. In addition to the tensile and LCF testing, the seeded materials were also subjected to a severe water quench test. This water quench test was developed to detect PPB in large volumes of material. This test has revealed defects as small as 8 mils^2 at quench crack fracture origins. An example of a PPB defect at quench crack origin is shown in Figure 9. In this study, none of the doped EX or EX+F Rene' 95 cracked while the HIP material cracked severely. Table V summarizes the water quench test results for this investigation.

Table III. Effects of Extrusion + Isothermal Forging
on the Tensile Properties of Doped Rene' 95

| | RT Average Properties | | Fracture Origins | |
Product	UTS (KSI)	% Elong	% Failed at PPB Defects	No. of Tests
HIP (Unseeded Baseline)	236	18	10%	10
HIP (Seeded)	208	8	100%	18
EX+F (Seeded)	235	18	0%	17

Table IV. Effects of Extrusion + Isothermal Forging on
the LCF Properties of Doped Rene' 95

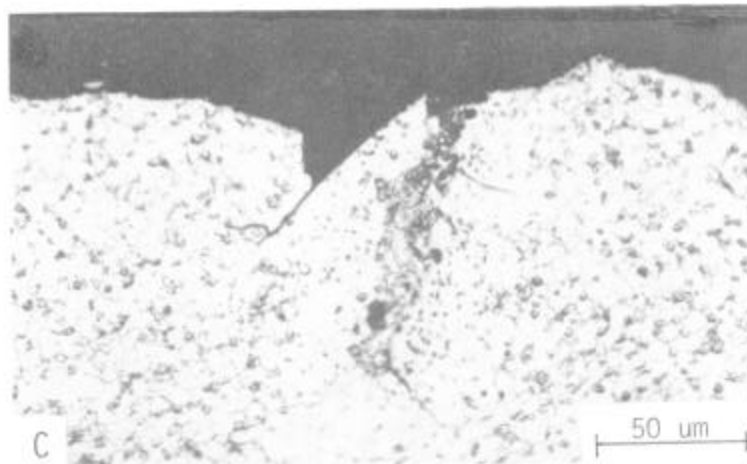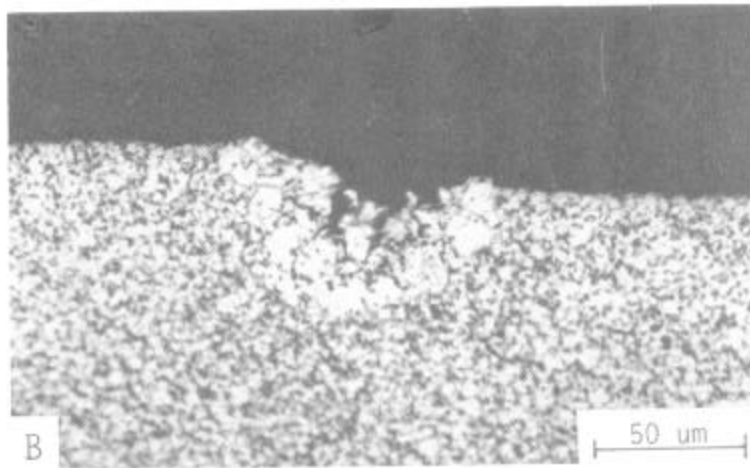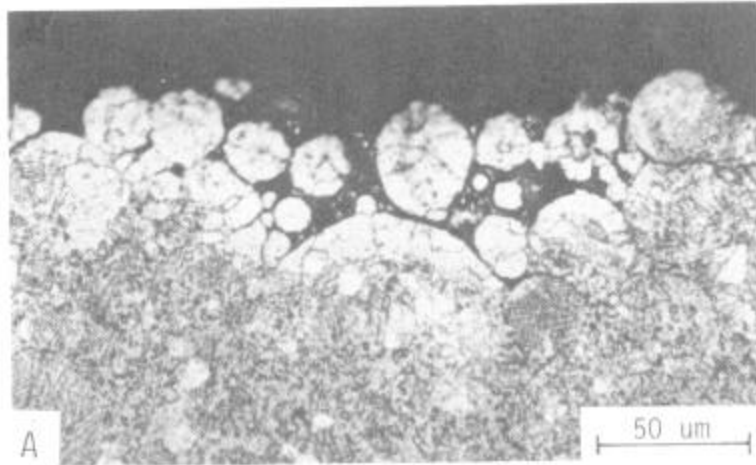|	Avg. LCF Life (Cycles)	% Failing at PPB	No. of Tests
HIP (Unseeded Baseline)	37000	5	826
HIP (Unseeded Material from the present study)	73299	11	9
HIP (Seeded)	8675	95	20
EX+F (Seeded)	53111	0	56

Figure 7 - Optical micrographs showing typical
microstructure of defects at LCF origins in
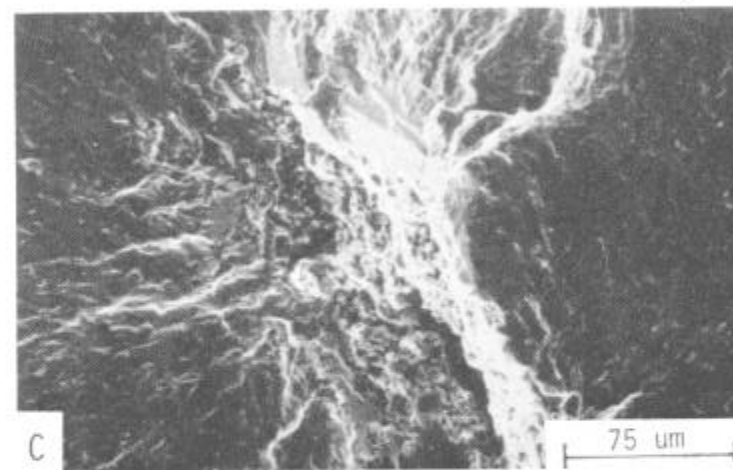doped Rene' 95 material.

A) HIP
B) As-Extruded
C) EX+F

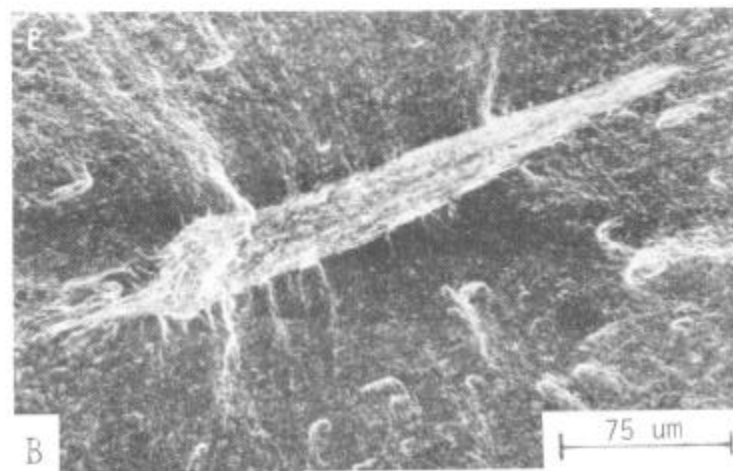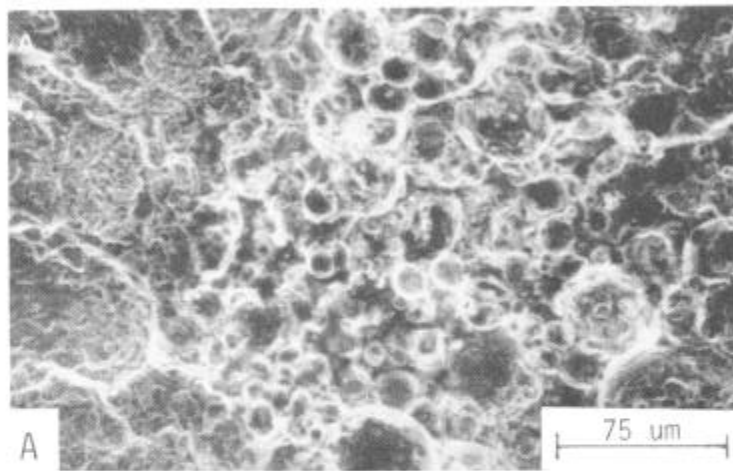Figure 8 - SEM fractographs of typical seeded defects observed at LCF origins in doped Rene' 95 material.
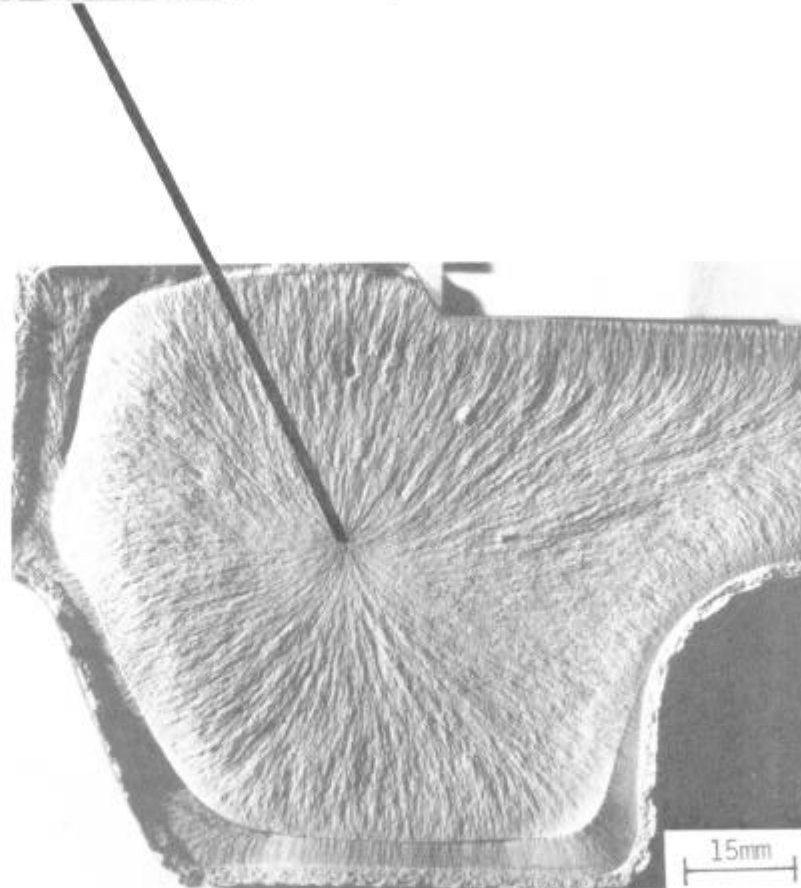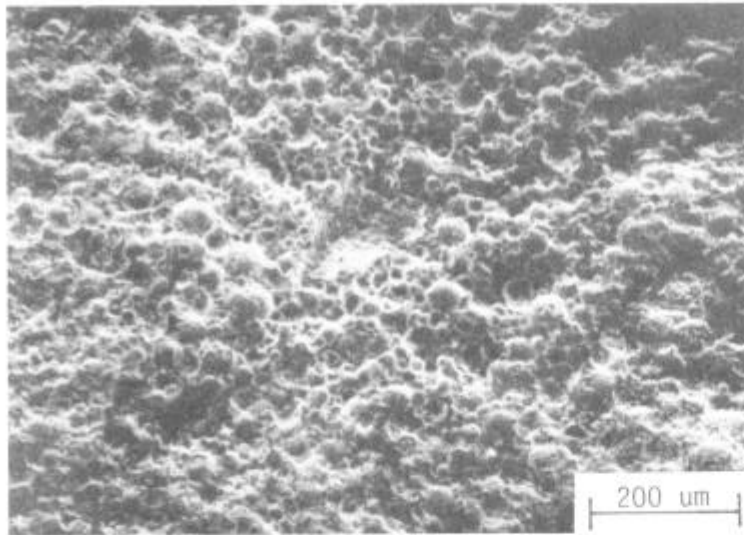
A) HIP
B) As-Extruded
C) EX+F

Figure 9 - Water quench test fracture micro-
graph showing PPB in crack initiation site of
doped HIP Rene' 95.

Table V. Results of Water Quench Tests for
Doped Rene' 95

Material Type

Seed Type	HIP	As-Extruded	EX+F
Buna N	3 major cracks; 400, 400, 704 mil^2 PPB defects at crack origin	Did not crack	Did not crack
Mill Scale	5 major cracks; 384, 484, 572 624, 900 mil^2 PPB defects at crack origins	Did not crack	Did not crack

Undoped Materials

Defect Type and Size. Table VI compares the defect type, size and failure locations of LCF specimens from HIP, H+F[3], and EX+F PM Rene' 95. In contrast to HIP specimens which invariable failed from impurity-related defects (Types 1 through 4), a number of TMP specimens failed from Type 5 origins which are crystallographic and do not contain impurity-related defects. A typical Type 5 defect is shown in Figure 10. These origins also show the regions of crack initiation and Stage 1 propagation as evident by the small facets delineating the initiation site. Consequently, initiations from a Type 5 defect are usually associated with long LCF life.
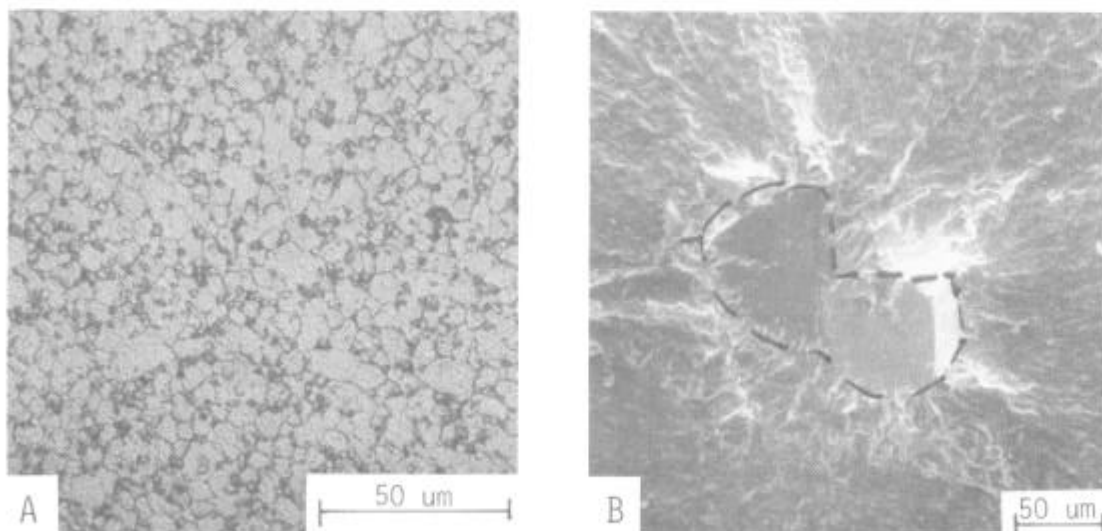

Figure 10 - Type 5 Crystallographic Defect.

A) Optical micrograph from a
   metallographic section
B) SEM fractograph of fatigue
   initiation site

Type 1 and Type 2 ceramic inclusions constituted the most frequently observed defects in all materials. The average size of each type (5-10 mils^2) did not differ significantly between all three materials, although the maximum sizes (especially Type 2) appear to be somewhat smaller in the TMP specimens. This suggests that the Type 2 defects may have been dispersed by TMP.

The Type 3 (PPB) defects were only infrequently found in the HIP material, much less in the H+F material with 60-80% forging reduction, and none were found in the EX+F material. In addition, the average and especially the maximum size of Type 3 defects found in the H+F specimens (4.2 and 4.5 mil^2) were considerably smaller than those found in the HIP specimens (19 and 242 mil^2). The frequency of failure from void defects (Type 4) was increased in the TMP specimens, 14-30% for H+F and 8-26% for EX+F at $\Delta\varepsilon_t$ < 0.75%,as compared with 1% or less for the HIP specimens. The lack of Type 4 failures in the latter case is not surprising since the relatively small voids would be bypassed as initiation sites in favor of the larger defects present. Once the larger defects had been dispersed by TMP, then the more abundant smaller defects would be favored for crack initiation.

Effect of Thermal Mechanical Processing on Low Cycle Fatigue

The LCF lives of HIP, H+F and EX+F materials are compared in Figure 11. The comparison shows that the lives of TMP materials are significantly better than those of HIP material. The LCF life improvement through TMP is related to the fatigue origin defect type and size as discussed below.

It was evident from the previous discussion and Table VI that TMP dispersed and reduced the size of defects. In addition, a larger percentage of TMP specimens failed from smaller Type 4 void defects (<2 mil^2) and Type 5 crystallographic origins. The reduced defect size and the lack of reactive defects resulted in the improved LCF life. The TMP materials generally had a very fine grain size which also helped improve the LCF life by retarding the initiation process.

The TMP specimens were much less prone to surface initiation. At 1000°F, 0.66% $\Delta\varepsilon_t$, very few failures at surface defects were observed. Under conditions more conducive to surface initiation (750°F/ $\Delta\varepsilon_t$ >0.75%), the frequency of surface failure was 33% for H+F, 15% for EX+F and 75% for HIP specimens.

Figure 12 compares the size of internal defects for EX+F material vs. HIP material as a function of LCF life. The internal defects observed (Type 1 and Type 2) are generally smaller for TMP material than HIP material. In addition, there is an improvement in LCF life for a given defect size. This suggests that the initiation and Stage 1 propagation periods for EX+F are longer than HIP material. A comparison was also made for surface initiated failure and the improvement was not as obvious.
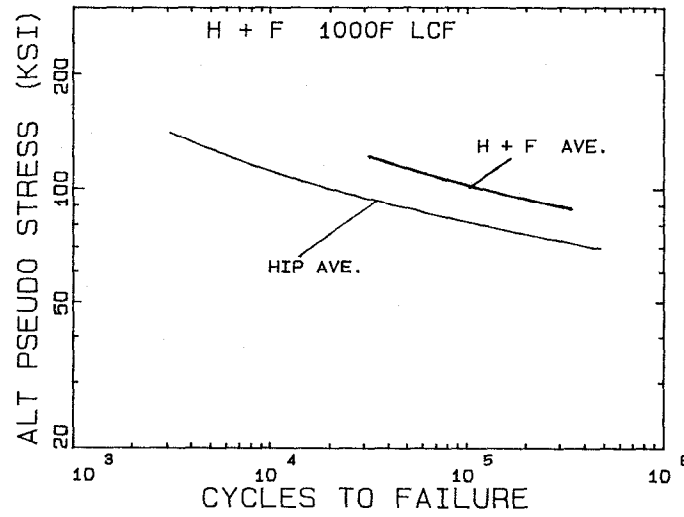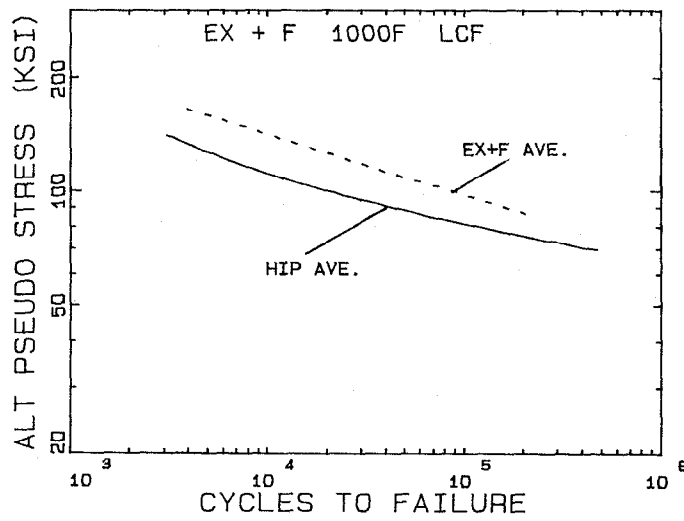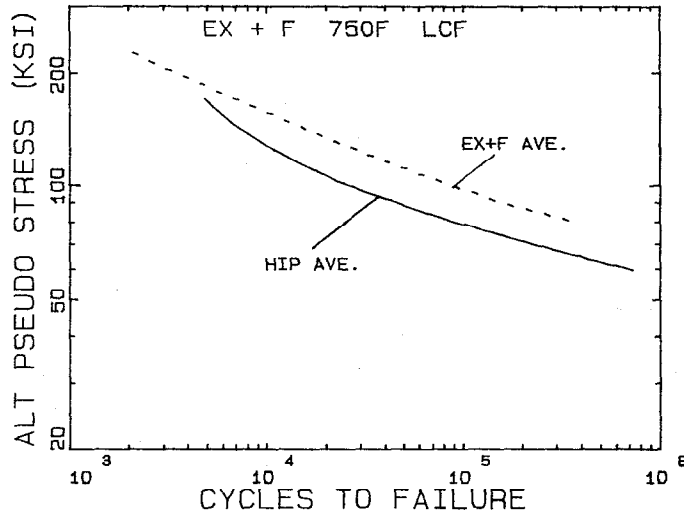
Figure 11 - Comparison of average LCF lives
of HIP vs. H+F and EX+F Rene' 95.

Table VI. Comparison of Defect Type and Size at LCF Initiation Site
HIP vs. H+F and EX+F

| TEMP °F	Δεt%	MATERIAL	NO. OF SURFACE FAILURES %	FREQUENCY OF DEFECT TYPE % 1	2	3	4	5	DEFECT TYPE	DEFECT SIZE, MILS² HIP AVE.	HIP MAX.	H+F AVE.	H+F MAX.	EX+F AVE.
1000	0.75	HIP	76	21	74	4	1	0	1	6.7	36	5.3	16.0	4.8
		H+F	5	66	5	0	0	29	2	9.5	50	6.1	11.2	8.9
		EX+F	37	75	25	0	0	0	3	18.7	242	None	None	None
									4	6.3	10.3	None	None	None
1000	0.75	HIP	31	15	77	7	1	0	1	11.2	50	3.9	12.0	4.8
		H+F	5	29	28	3	14	26	2	13.1	111	4.8	13.0	7.1
		EX+F	4	38	54	0	8	0	3	19.3	83.6	4.2	4.5	None
									4	5.3	6.8	0.8	1.4	1.0
750	0.75	HIP	75	33	58	9	0	0	1	7.5	9.1	6.4	13.7	4.1
		H+F	33	13	24	0	30	33	2	8.6	13.1	4.2	9.3	5.2
		EX+F	15	32	39	0	26	3	3	--	6.4	None	None	None
									4	None	None	1.1	1.5	0.5

263
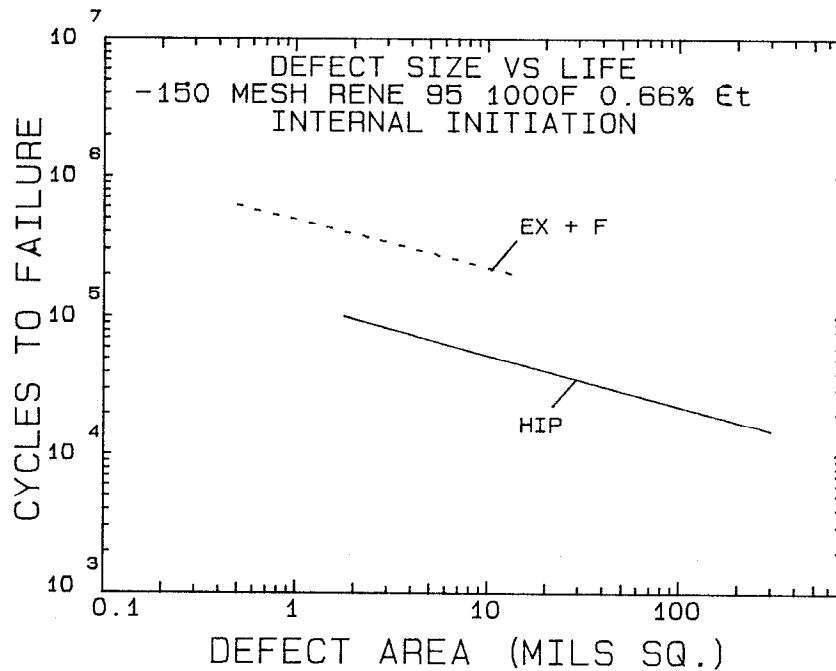
Figure 12 - Internal initiated defect size vs. LCF of HIP and EX+F Rene' 95 tested at 1000°F 0.66% ε_t.

A similar improvement in LCF life for TMP materials was observed by Minor and Gayda[7]. They investigated the LCF behavior of HIP, EX+F and cast plus wrought Rene' 95. Figure 13 shows the LCF comparison at 1200°F. At high strain ranges the LCF lives of all three materials are similar, while at strain ranges less than 1.0% the EX+F shows the longest LCF life. Their study also confirmed that the EX+F material was more prone to internally initiated failure.
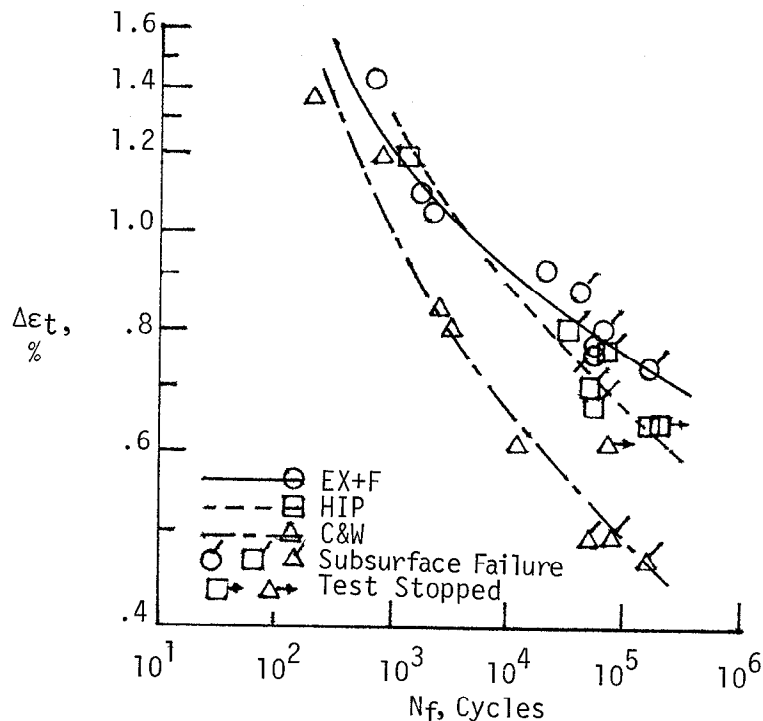

Figure 13 - Cyclic life - total strain range of Rene' 95 at 1200°F.

Processing, Microstructure and Mechanical Properties of Extruded plus Isothermally Forged PM Rene' 95

The first full-scale EX+F Rene' 95 gas turbine engine components were processed to the disk configuration shown schematically in Figure 14. This shape was obtained by isothermally forging a six inch diameter extrusion at 2000°F to a minimum height reduction of 70%. Figure 15 shows the typical fine recrystallized grain structure for three disk locations. The average grain size measured ASTM 11-12.

A preliminary investigation was conducted on sample disk material to study the effects of heat treatment on mechanical properties. The selected heat treatments were:

A) 2050°F/1 hr./salt quench + 1600°F/1 hr./air cool + 1200°F/24 hrs./air cool.

B) 2000°F/1 hr./oil quench + 1400°F/16 hrs./air cool.

and C) 2050°F/1 hr./air cool + 1400°F/16 hrs./air cool.

The "solution" temperature in each of these heat treatments is below the γ' solvus (approximately 2120°F). This prevented the extensive grain coarsening associated with complete solutioning of the γ' phase. It is well known[8][9] that the properties of γ' strengthened nickel-base alloys like Rene' 95 are sensitive to cooling rates from the solution temperature. Since the cooling rate is controlled by the thickness of the component, this can result in non-uniform mechanical properties in components having complex thick and thin cross-sections. The heat treatment conditions listed above were selected to produce a variety of strengths and structures, thereby simulating the sections of various components. Experimental heat treatment C was selected to study mechanical properties for slow cooled, thick section components.
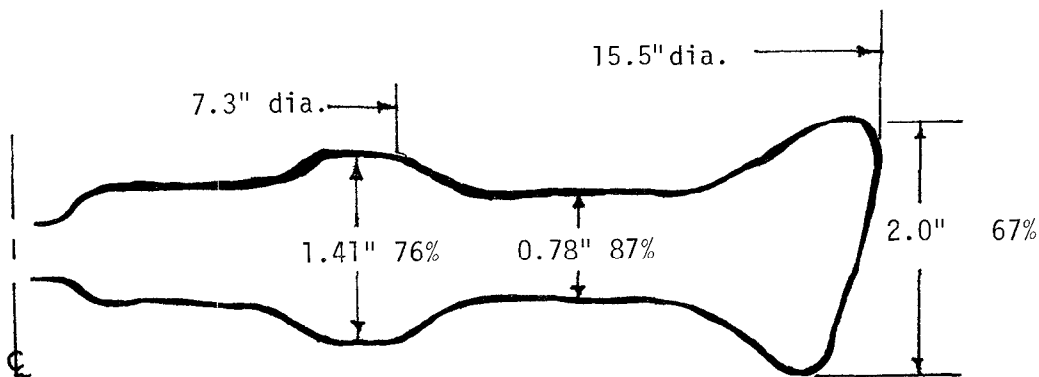

Figure 14 - EX+F Rene' 95 disk dimensions and forge reductions.
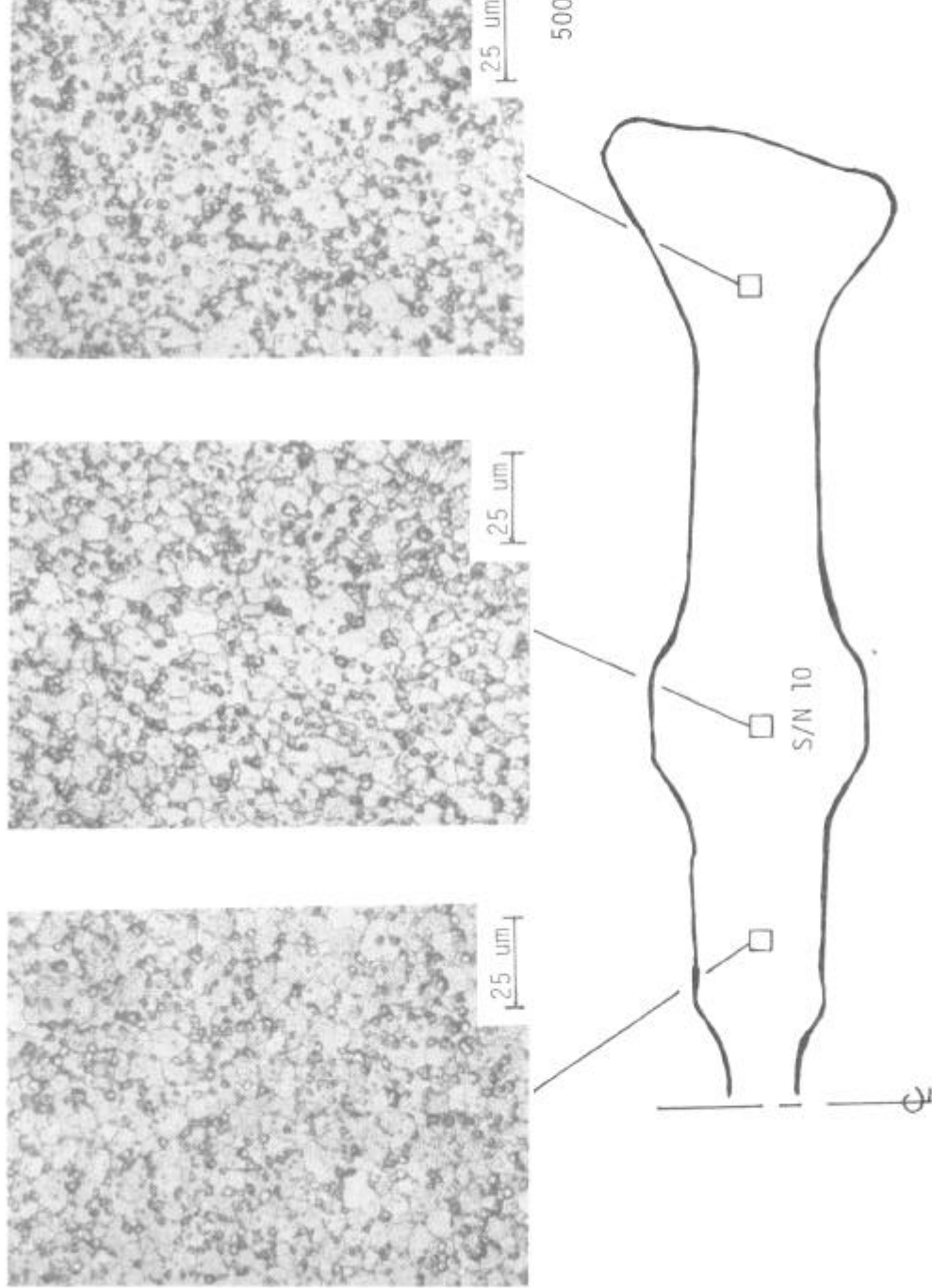
Figure 15 – Mid-thickness microstructures for EX+F Rene' 95 disk.

The TEM replica technique was used to evaluate the γ' characteristics for these three heat treatment conditions. Figure 16 shows TEM replica micrographs which illustrate their primary and intermediate γ' features. The primary γ' sizes were similar and ranged from one to three microns in size. The volume fraction, however, increased with decreasing solution temperature. The intermediate γ' forms on cooling from the solution temperature. The more rapid the cooling, the finer the size and distribution. Heat treatment C, air cooled from the annealing temperature, resulted in the largest intermediate γ', measuring approximately 0.2 microns in size. The quenched materials had smaller intermediate γ' measuring approximately 0.05 microns in size.

Specimens from each heat treatment condition were prepared for a tensile, rupture and creep property comparison. Figure 17 shows the tensile data obtained for room temperature and 1200°F test conditions. The data show that slow cooling results in lower strength but higher ductility. The ductility of all three heat treatments is generally better than HIP Rene' 95 heat treated to similar strength levels.

The rupture and creep specimens were tested at 1200°F using initial stresses of 150 ksi for the rupture evaluation and 123 ksi for the creep evaluation. The results are provided in Table VII. The trends in rupture and creep strength are consistent with that observed from the tensile study, that is, a slow cooling rate results in lower creep and rupture.

This study showed that the tensile, rupture and creep properties can be controlled by heat treatment. The strengths obtained for experimental heat treatment C, although lower, were nevertheless encouraging relative to the requirements of most thick sectioned components.

Table VII.   EX+F Rene' 95 Disk Heat Treat Study
Creep and Rupture Test Data

Forging S/N	Location/ Orientation	Temp. (°F)	Stress (KSI)	Total Percent Strain @ 50 Hrs.	Rupture Life (Hrs.)	Heat Treat.(1)
1	Rim-Tang.	1200	150	---	85.2	A
1	Rim-Tang.	1200	123	0.02		A
2	Rim-Tang.	1200	150	---	107.7	B
2	Rim-Tang.	1200	123	0.02		B
3	Rim-Tang.	1200	150	---	18.6	C
3	Rim-Tang.	1200	123	0.16		C

(1) Heat Treatments: A = 2050°F/1 Hour/Salt Quench
1600°F/1 Hour/Air Cool + 1200°F/
24 Hours/Air Cool

B = 2000°F/1 Hour/Oil Quench
1400°F/16 Hour/Air Cool

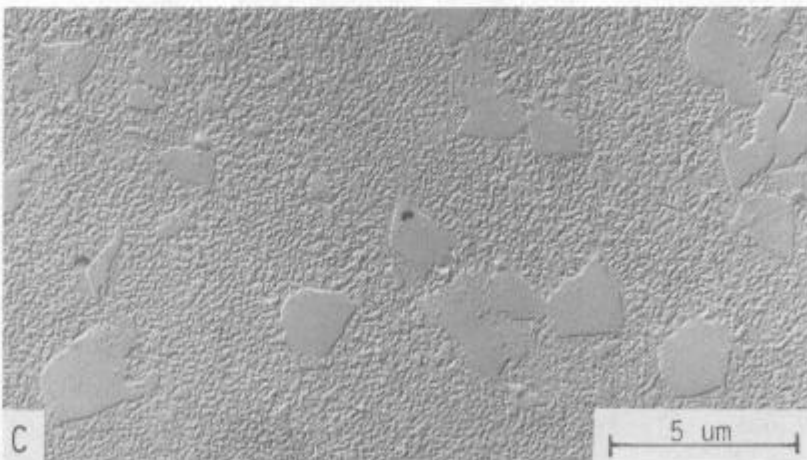C = 2050°F/1 Hour/Air Cool
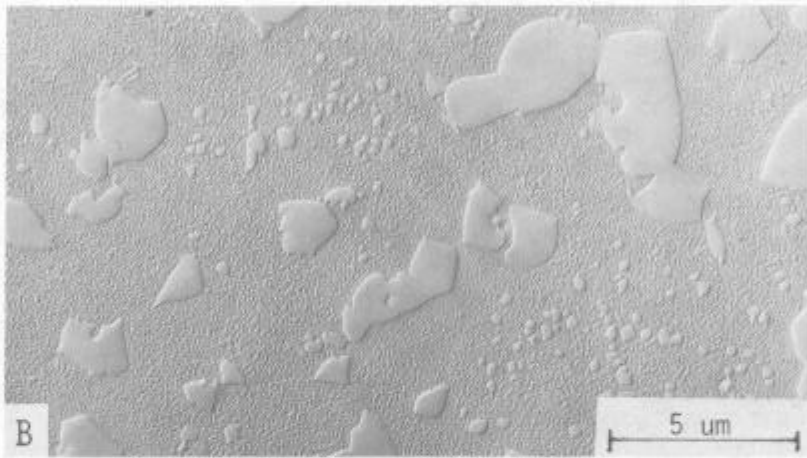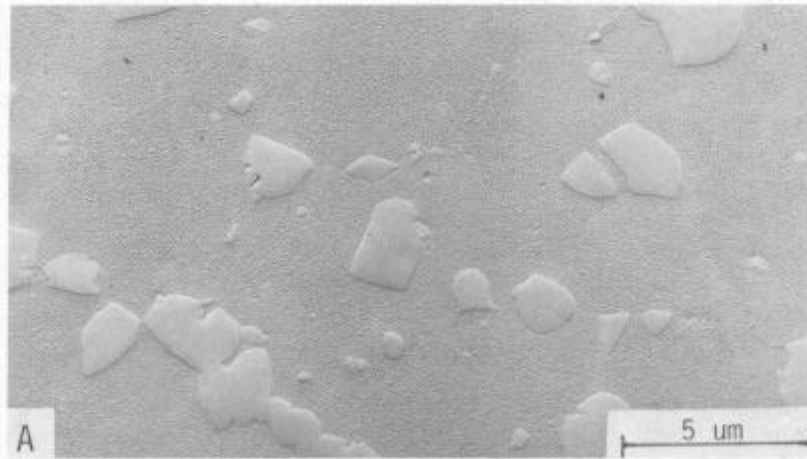1400°F/16 Hours/Air Cool

Figure 16 - TEM replications showing the effect of heat treatment on γ' size.

A) 2050°F/1 hr/salt + 1600°F/1 hr/AC + 1200°F/1 hr/AC

B) 2000°F/1 hr/oil + 1400°F/16 hr/AC

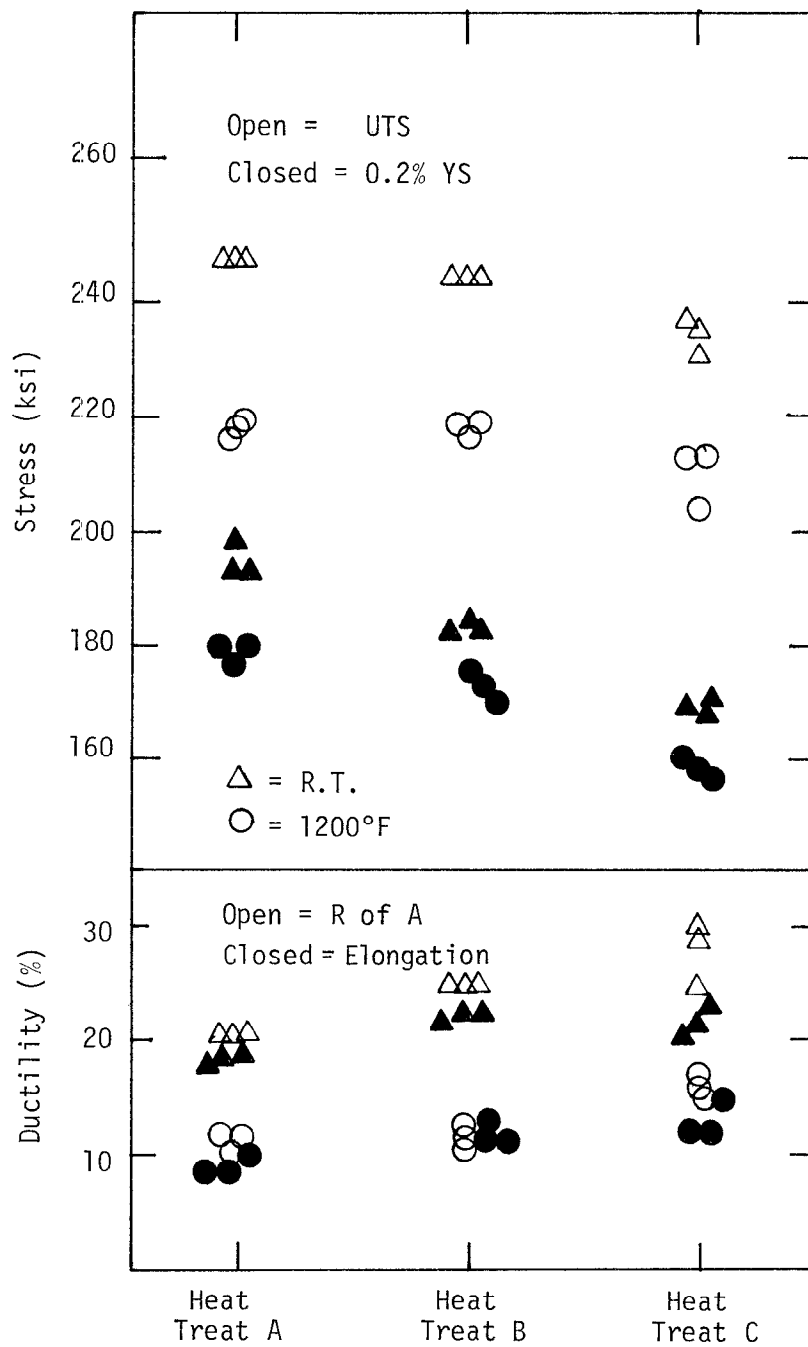C) 2050°F/1 hr/AC + 1400°F/16 hr/AC

Figure 17 -- EX+F Rene' 95 disk heat treat study tensile results.

Additional tests were conducted to characterize the LCF and fatigue crack growth characteristics. Since these properties are most critical in thick section bore regions of high pressure turbine disks, heat treatment C was selected for this evaluation. The LCF specimens were tested at 750 and 1000°F for $\Delta \epsilon_t$ = 0.66, 0.70 and 0.78% and A = 1.0 conditions. The average fatigue lives, shown in Figure 11, well exceed the typical HIP curves. The fatigue origins of each LCF specimen were also characterized. None of the fatigue origins consisted of PPB Type 3 defects. Failures initiated at Type 1 and 2 ceramics or Type 4 pores ranged from less than 1 mil^2 to approximately 11 mils^2. The low life specimens failed at surface located origins, while the higher life specimens failed at internal initiation sites.

Stage II fatigue crack growth rate data were generated at 750° and 20 cpm using the K_B bar specimen geometry developed by Coles et al[10]. Tests were also conducted on HIP PM Rene' 95 specimens obtained from a high pressure turbine disk for comparison. Crack growth was monitored with a DC potential drop testing monitoring technique[11]. The results for two tests per material are shown in Figure 18, and the difference in fatigue crack growth rates is negligible. Since the Stage II propagation rates are similar, this also suggests that the improvemment in LCF life for TMP Rene' 95 results from longer initiation and Stage 1 propagation periods.

Based on this investigation, a number of components have been successfully manufactured with the EX+F technique. The trends in mechanical property response to heat treatment identified in this study have been applied and successfully controlled.
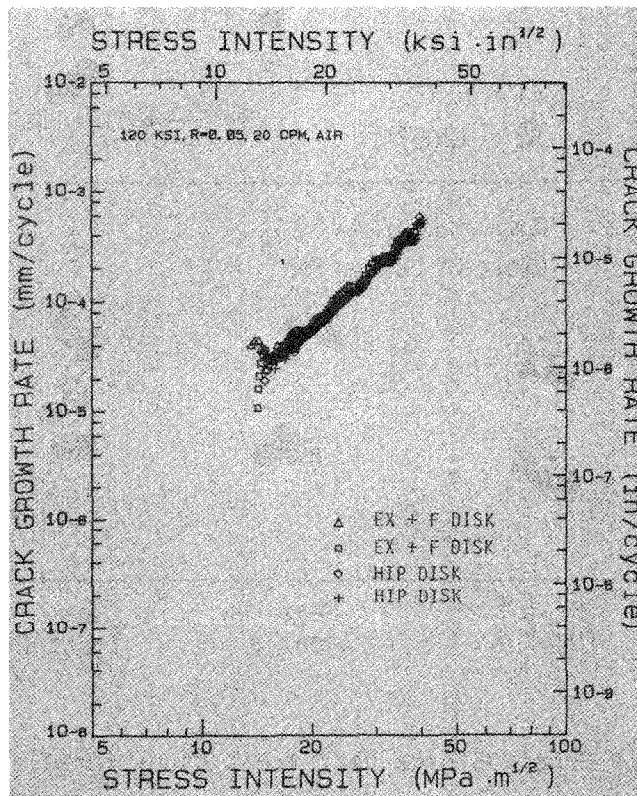

Figure 18 - EX+F and HIP Rene' 95 750°F
fatigue crack growth rates.

Conclusions and Future Directions

Results from the investigations referenced in this paper have demonstrated that TMP can significantly reduce and disperse defects thereby improving the LCF properties of nickel base PM superalloys. It has also been demonstrated that the detrimental effects of large reactive defects (PPB) can be eliminated by certain TMP techniques. The refined grain size of TMP material also enhanced the ultrasonic inspectability. This permits more stringent quality control practice. These combined improvements permit industry to place further confidence in the reliability and integrity of high strength PM superalloys.

However, the LCF lives of TMP PM material are still limited by Type 1 and Type 2 ceramic inclusions. Substantial additional component life benefits can be realized, but much further effort is required to reduce or eliminate these defects. This can be achieved by using clean melted input stock material followed by a ceramicless powder atomization process. Programs sponsored by various government agencies and industries are in place to develop clean melting and clean powder processes. Preliminary results from these developments[12][13] have been encouraging. Since the LCF life is also limited by surface initiated failure, surface enhancement techniques which are capable of generating a surface compressive stress layer to inhibit surface failure should be applied. This concept has been effectively demonstrated by a number of investigators[14][15]. Alloy development activities to modify composition and improve the intrinsic defect tolerance of the materials are also needed. These compositional modifications must consider and balance all other properties for engine applications. Programs [16][17] have been initiated to address this challenging goal.

Powder metallurgy technology is a cost effective means to produce highly alloyed compositions with the desired mechanical properties. As powder quality, availability and manufacturing techniques improve, implementation is expected to increase significantly. For jet engine applications, powder superalloy usage is projected to increase to meet the higher property and life requirements of future engines.

Acknowledgements

References

1. Private Communication, E. Hall, Corporate Research and Development Center, General Electric Company, September, 1982.

2. C.E. Shamblen and D.R. Chang, "Effect of Inclusions on LCF Properties of As-HIP Rene' 95", paper presented at TMS Fall Meeting - High Temperature Alloys Committee of AIME, Philadelphia, Pa., October, 1983.

3 W.H. Chang, H.M. Green, and R.A. Sprague, "Defect Analyses of P/M Superalloys", Rapid Solidification Processing Principles and Technologies III, Ed. R. Mehrabian, Proceedings of the Third Conference on Rapid Solidification Processing, Bureau of Standards, December 8, 1982, pp. 500-509.

4. Private Communication, M.F. Henry, Corporate Research and Development Center, General Electric Company, September, 1981.

5. S. Floreen and R.H. Kane, "An Investigation of the Creep-Fatigue-Environmental Interaction in a Ni-Base Superalloy", INCO Research and Development Center, Technical Paper 1020-T-OP, Suffern, New York, August, 1979.

6. L.F. Coffin, "The Effect of High Vacuum on Low Cycle Fatigue Law", Met. Trans., 3, 1972, pp. 1777.

7. R.V. Miner, J. Gayda, "Effects of Processing and Microstructure on the Fatigue Behavior of the Nickel-Base Superalloy Rene' 95", paper presented at TMS Fall Meeting - High Temperature Alloys Committee of AIME, Philadelphia, Pa., October 3, 1983.

8. C.E. Shamblen, R.E. Allen, and F.E. Walker, "Effect of Processing and Microstructure on Rene' 95", Met. Trans., 6A, November, 1975, pp. 2073-2082.

9. R.H. VanStone, "Processing Effects on Microstructure and Fatigue Properties of Nickel-Base Superalloys", Final Report, NADC 80124-60, General Electric Company, December, 1980.

10. A. Coles, R.E. Johnson, and H.G. Popp, "Utility of Surface Flawed Tensile Bars in Cyclic Life Studies", J. Eng. Mat. Tech., 98, 1976, pp. 305.

11. R.P. Gangloff, "Electrical Potential Monitoring of Crack Formation and Subcritical Growth from Small Defects", Fatigue of Engineering Materials and Structures, 4, 1981, pp. 15.

12. C.E. Shamblen, S.L. Culp, and R.W. Lober, "Superalloy Cleanliness Evaluation Using the EB Button Melt Test", Proceeding of the Conference Electron Beam Melting and Refining State of Art 1983, Ed. R. Bakish, Library of Congress ISSN 0740-8706, November 6-8, 1983, pp. 61-94.

13. E.E. Brown, J.E. Stulga, L. Jennings, and R.W. Salkeld, "The Influence of VIM Crucible Composition, Vacuum Arc Remelting, and Electro Slag Remelting on the Non-Metallic Inclusion Content of MERL-76", Superalloys 1980, Eds. J.K. Tien, et al., American Society for Metals, Metals Park, Ohio, 1980, pp. 159-168.

14. W. Renzhi, "Shot Peening of Superalloy and its Fatigue Properties at Elevated Temperature", First International Conference on Shot Peening, Paris, September, 1981, Pergomon Press, Oxford, pp. 395.

15. B.D. Boggs and J.G. Byrne, "Fatigue Stabiity of Residual Stress in Shot Peened Alloys", Met. Trans., 4, September, 1973, pp. 2153-2157.

16. J.C. Williams and J.P. Hirth, "Microstructure-Property Relations and Their Role in RSP Materials", Ibid. 3, pp. 135-149.

17. A.M. Adair, L.A. Jacobson, E.C. VanReuth, and J. Dickson, "Rapid Solidification - Past Promises and Current Reality," Ibid. 3, pp. 609-614.